Solution preparation

Tris–HCl buffer (10 mM, pH 7.4) containing 0.1 M NaCl was selected to keep the pH value and maintain the ionic strength of the solution. BSA solution (0.029 mM) was prepared in Tris-HCl buffer and stored in a refrigerator. Standardization of the BSA solution was done spectrophotometrically at 279 nm using the extinction coefficient (ε = 43824 M^{-1} cm^{-1}). The stock solution of PAs and FLs (1.5 mM) were prepared by directly dissolving them in ethanol.

Fluorimetric titration

The fluorescence quenching method was used to investigate the interactions of PAs and FLs with BSA. All spectra measurements were obtained using a luminescent spectrometer (LS-55, Perkin Elmer) at three different temperatures (292, 303, and 310 K). The solution of BSA (2 mL, 0.029 mM) was titrated in cuvette by successive addition of individual phenolics solution aliquots (10μL) from a stock of 1.5 mM. The emission spectra were recorded in the wavelength range of 300–400 nm, while a fixed wavelength of 279 nm was used for the excitation. The excitation and emission slit widths were set to 10 nm and the scanning speed was 500 nm/min (Jin, Wei, Qi, *et al*., 2012). The synchronous fluorescence spectra were obtained by synchronous scanning at the wavelength range of 250–350 nm, with the wavelength interval ($\Delta\lambda$) at 15 and 60 nm, at which the spectrum only shows the spectroscopic behavior of Tyr and Trp residues of BSA, respectively (Lloyd and Evett, 1977). The three-dimensional (3D) fluorescence spectrum of BSA and the BSA–PA/FL (60 μL) complexes at 292 K were performed under the following conditions: the excitation scan range of 200–350 nm in 10 nm increments, and the emission spectrum was set as between 200 and 500 nm (Zahirović, Žilić, Pavelić *et al*., 2019). The number of scanning curves was 16, and other scanning parameters were the same as the fluorescence quenching spectra.

Thermal denaturation

Simultaneous monitoring of the PAs and FLs at 330 nm and 350 nm during the thermal conversion of purified albumin was carried out using nanoscale differential scanning fluorimetry (nanoDSF) with an excitation wavelength of 280 nm. The capillaries were filled with albumin (2 μM) and PA/FL (7.8 μM), placed into the sample holder and the temperature was increased from 297 to 368 K with a temperature gradient of 1K/min, with one fluorescence measurement per 0.2 K (Magnusson *et al*, 2019). The ratio of the recorded emission intensities (Em_{350nm}/Em_{330nm}), which represents the change in Trp fluorescence intensity, was plotted as a function of the temperature. Additionally, their first derivative was calculated with the manufacturer's software, displaying as the peak at the point of the maximal slope, which corresponds to the unfolding transition temperature (T_m) which is defined as the temperature at which half of the protein is unfolded and acts as an important parameter for the conformational stability of a protein.

Computational studies

Density function theory (DFT)

Density function theory (DFT) is a computational modeling study used to investigate the electronic structure of molecules. Quantum chemical calculations were performed at the B3LYP level with a 3-21G basis set using ORCA 5.0. software (Neese, 2022). All compounds were first optimized using Avogadro software. Relevant energetic properties such as the dipole moment and energy were calculated for each compound. Frontier molecular orbitals (FMO) studies can be used to predict the chemical reactivity of compounds and identify their most likely reactive sites. Two important parameters that quantitatively describe these interactions are the energy of HOMO and LUMO. The calculated EHOMO and ELUMO energies of compounds help to explain global reactivity descriptors that influence the nature of the interaction. Additionally, the chemical reactivity parameters such as electronegativity (χ), chemical potential (μ), global electrophilicity index (ω), global hardness (η) and global softness (*S*) were calculated.

Docking study

Docking process were carried out using Autodock Vina (Trott and Olson, 2010). Phenolic acids and flavonoids have been optimized and exported to a pdf file. Non-polar hydrogens were merged, rotatable bonds were defined and torsional bonds of ligand were set free. Protein 3D structure of bovine albumin serum (BSA) was acquired form Protein Data Bank (PDB code 4F5S) (Bujacz, 2012). Polar hydrogens, Kollman charges and solvent parameters were added. The binding site were defined using grid size coordinates of 94x67x90 and grid center coordinates of x=72, y=27, z=92 with a grid space of 0.375 Å (Bautista-Aguilera *et al.,* 2014). For the visualization of the docking results was used PyMOL software (DeLano, 2002).

RESULTS AND DISCUSSION

Quenching constant and bonding parameters

Fluorescence quenching has proven to be a very sensitive technique with many capabilities to analyze the interaction between ligands and proteins (local changes in the polarity, conformation, and/or exposure to the solvent). The interaction will lead to modifications in fluorescence intensity-decrease ('quenching') or an increase ('enhancement') of protein. Bovine serum albumin has an emission maximum at 348 nm under excitation at 279 nm mainly because of the presence of Trp residue. It was found that the fluorescence intensity of BSA is gradually decreasing with increasing concentration of selected PAs and FLs as a function of the level of BSA modification by the attachment of the ligands (Figure 2). SA with BSA shows *isosbestic point* which indicates the formation of a stable protein-ligand complex. The *isosbestic point* shows the equilibrium dissociation reaction of the complex and is independent of the reactant concentration.

The quenching mechanism for interacted molecule was analyzed according to the Stern-Volmer equation (1):

$$\frac{F_0}{F} = 1 + k_q\tau_0 = 1 + K_{SV}[Q] \qquad (1)$$

where F_0 is the fluorescence intensity in the absence of the quencher, F is the fluorescence intensity in the presence of the quencher, [Q] is the ligand concentration, and k_q the quenching constant for a bimolecular reaction, K_{SV} the Stern-Volmer constant, and τ_0 the average lifetime for fluorophore without a quencher. The above equation is applied to determine quenching constants (k_q and K_{SV}) by linear regression of a plot of F_0/F against [Q]. The binding constant for ligand-protein interaction (K_b) and the binding site number for BSA (n) were calculated by equation (2) for the equilibrium between free and bound molecules.

$$\log\frac{F_0 - F}{F} = \log K_b + n\log[Q] \qquad (2)$$

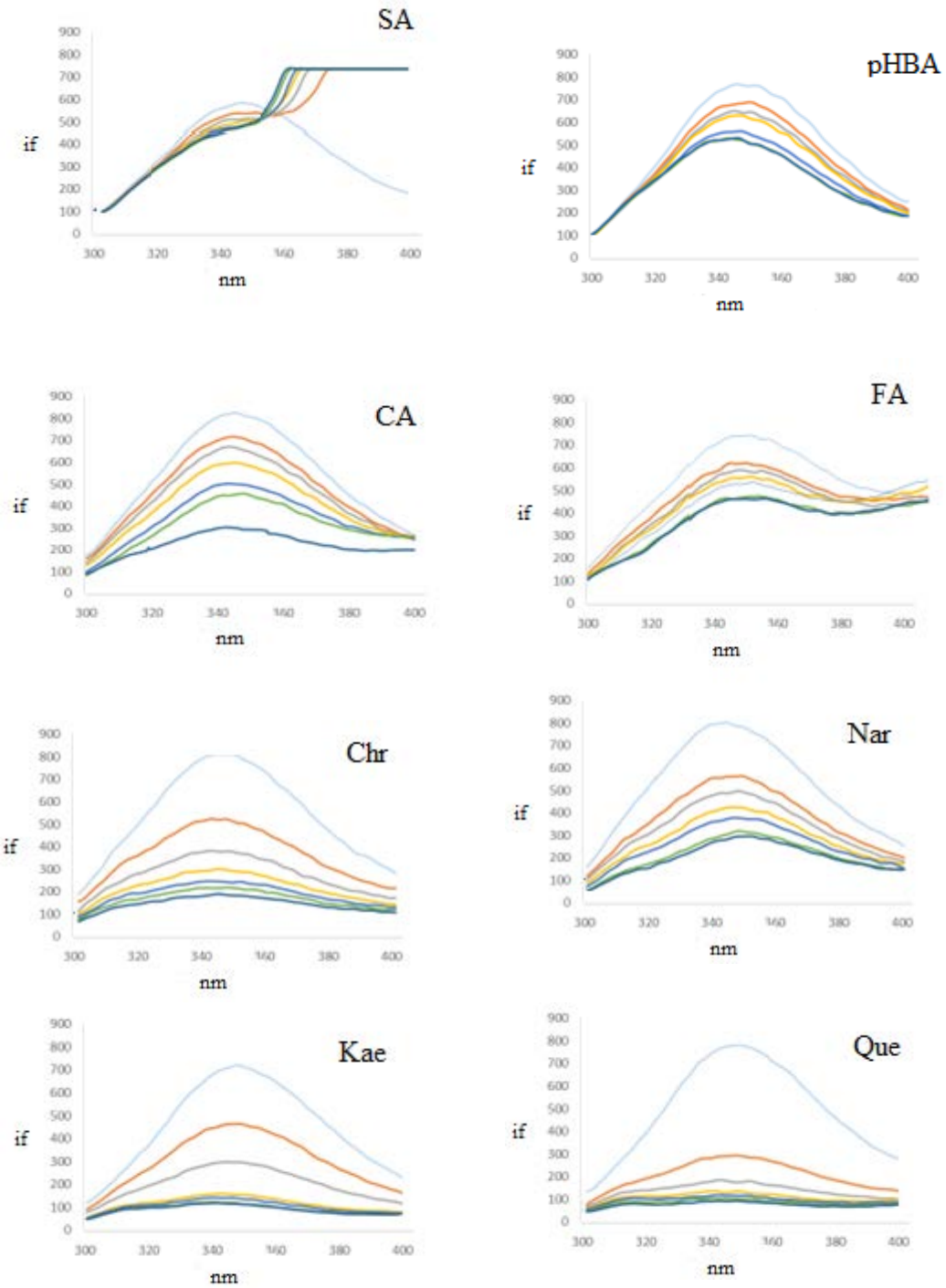

Figure 2: Fluorescence quenching of BSA by selected PAs and FLs. From the top to bottom the values of Pas/FLs concentration were 0, 2.5, 5.0, 7.4, 9.9, 12.2, and 14.6 μM, respectively, T = 292 K

The values of K_b and n could be determined from the intercept and slope by plotting log $(F_0\text{-}F)/F$ against log[Q]. The quenching constants and binding parameters for BSA by four different PAs are summarized in Table 1. Values for bimolecular quenching constants (k_q) reflect quenching or the accessibility of the fluorophores to the quencher. Fluorescence quenching mechanism may result from a variety of processes such as excited state reactions, molecular rearrangements, energy transfer, ground-state complex formation (static quenching), or collisional interactions (dynamic quenching), (Lakowicz, 2013). Static quenching refers to the formation of the fluorophore quencher complex in the ground state; whereas dynamic quenching refers to a process where the fluorophore and the quencher interact during the excited-state lifetime of the fluorophore. The values of k_q are two orders of magnitude greater than the maximum diffusion collision quenching constant (~10^{10} M^{-1} s^{-1}) and can be assumed that the quenching mechanism was due to complex formation between BSA and PAs/FLs (a static mechanism), rather than dynamic collision (Bose, 2016).

Table 1: Quenching constants and binding parameters for BSA-PAs/FLs complexes

BSA-PAs/FLs	T (K)	$K_{SV}\times10^4$ (M^{-1})	k_q*$\times10^{12}$ (M^{-1} s^{-1})	K_b (M^{-1})	n
BSA-SA	292	1.07	2.14	9.52×10^1	0.53
	303	3.46	6.93	7.04×10^3	0.83
	310	4.70	9.41	1.58×10^3	0.70
BSA-pHBA	292	2.85	57.10	2.50×10^3	0.77
	303	6.59	13.10	3.96×10^3	0.78
	310	4.11	8.22	2.74×10^2	0.55
BSA-CA	292	3.45	6.91	1.83×10^6	1.28
	303	3.87	7.74	4.99×10^2	0.53
	310	7.33	14.60	2.13×10^4	0.85
BSA-FA	292	10.15	23.00	7.17×10^2	0.64
	303	9.14	18.20	9.53×10^2	1.02
	310	1.26	25.20	8.51×10^2	1.21
BSA-Chr	292	46.00	23.00	$2.59\text{x}10^5$	1.00
	303	24.90	14.10	$5.78\text{x}10^3$	0.73
	310	16.66	8.32	$1.14\text{x}10^4$	0.81
BSA-Nar	292	21.20	10.60	$1.22\text{x}10^4$	0.80
	303	42.30	21.10	$1.69\text{x}10^6$	1.21
	310	33.70	16.80	$2.56\text{x}10^5$	1.05
BSA-Kae	292	79.30	39.60	$1.66\text{x}10^7$	1.32
	303	3.27	16.30	$1.80\text{x}10^6$	1.26
	310	2.82	14.10	$1.47\text{x}10^4$	0.82
BSA-Que	292	85.60	42.80	$6.27\text{x}10^4$	0.81
	303	39.30	19.60	$4.35\text{x}10^4$	1.30
	310	57.00	28.50	$1.28\text{x}10^4$	0.93

*The quenching constant (k_q) were calculated using equation $k_q = K_{SV}/\tau_0$, τ_0 is taken as 5×10^{-9} s

BSA-Que complex and BSA-*p*HBA showed stronger quenching constants (k_q) at 292 K (42.80×10^{12} M^{-1} s^{-1} and 57.10×10^{12} M^{-1} s^{-1}, respectively). This effect was probably dependent upon the position and number of the hydroxy group. The intensive quenching ability has Kae to the BSA. Also, the presence of the methoxy group seems to be important for quenching activity too. The k_q value for BSA-FA was slightly lower than the k_q of BSA-*p*HBA.

The temperature rises could decrease the quenching constant because of the lower stability of the ligand-BSA complex, while they could increase the dynamic quenching constant due to the increased possibility of diffusivity of the molecules and molecular collision. The values of the Stern-Volmer constant *(K_{SV})* at different temperatures were shown in Table 1. The results for BSA-PAs interaction showed that the K_{SV} will increase with increasing temperature, aside from the *K*sv values for the BSA-FA decrease with the increasing temperature which coincides with the static form of the hardening mechanism. Data obtained for hydroxycinnamic acids systems in this study corresponded with these findings by other authors (Trnkova, Bousova, Kubicek, *et al*, 2010). The results for the interaction between BSA and FLs showed an increase in the BSA-Nar complex and a decrease in the BSA-Chr and BSA-Kae complexes, while the BSA-Que complex showed an irregular change in Ksv values. These values are consistent with the results in the literature (Wang, Qin, Chang, *et al,* 2018).

The binding constant K_b reflects the power of ligand-protein association and thus can be used for comparison of binding affinities of structurally-related ligands to protein molecule connected with alteration of its secondary structure. It was demonstrated that the interaction of PAs/FLs with protein molecule depends mainly on the size and structure of the ligand, especially on the number and position of hydroxy groups on the aromatic ring (Bartolomé, Estrella, and Hernandez, 2000). The binding constant (K_b) for BSA-PAs interaction was ranked in the order BSA-CA > BSA-*p*HBA > BSA-FA > BSA-SA. BSA-CA system showed a significant binding constant which confirms the significance of hydroxy groups in the process of binding. The same constant for the interaction of FLs with BSA was ranked in the order BSA-Kae > BSA-Nar > BSA-Que > BSA-Chr. Also, in these interactions with BSA there was a significant impact of hydroxy groups in ligands.
The binding site number shown in Table 1 ranged between 0.53 and 1.32 (at 292 K) suggesting that nearly one molecule of tested phenolics was associated with BSA. Kaemferol, with four hydroxy groups on rings has the highest value.

Thermodynamic parameters

Thermodynamic parameters are important for the noncovalent acting forces and they are used to determine the type of interaction between ligand and protein. Utilizing the binding constant K_b, the free energy change (ΔG) enthalpy (ΔH), and entropy (ΔS) values can be estimated from the van't Hoff and thermodynamic equations:

$$\ln\frac{K_{b1}}{K_{b2}} = \left(\frac{1}{T_1} - \frac{1}{T_2}\right)\left(-\frac{\Delta H}{R}\right) \quad (3)$$

$$\Delta G = -RT\ln K_b \quad (4)$$

$$\Delta G = \Delta H - T\Delta S \quad (5)$$

where T is the temperature and R the universal gas constant. The equation (4) is applied to determine the value of ΔG, while ΔS and ΔH could be determination from the intercept and slope by plotting ΔG against T. Hydrophobic (ΔH >0 and ΔS>0), electrostatic (ΔH<0 and

$\Delta S>0$), Van der Waals and hydrogen bonds ($\Delta H<0$ and $\Delta S<0$) interaction are the main forces. The negative values of ΔG were indicating a spontaneous process of binding for interaction between BSA and PAs/FLs. Hydrogen bonding and Van der Waals forces played a major role in the interaction of BSA with *p*BHA, CA, Chr and Kae while hydrophobic bonds were found in the interaction of BSA with SA, FA, Nar and Que. (Table 2).

Table 2: Thermodynamic parameters for BSA-PAs/FLs complexes

#	ΔG (kJ mol^{-1}) (T (K))	ΔH (kJ mol^{-1})	ΔS (J mol^{-1} K^{-1})
BSA-SA	-11.06 (292 K) -22.32 (303 K) -18.99 (310 K)	135,06	505,38
BSA-*p*HBA	-19.00 (292 K) -20.88 (303 K) -14.48 (310 K)	-79.82	-204.43
BSA-CA	-35.03 (292 K) -15.65 (303 K) -25.70 (310 K)	-233.48	-656.10
BSA-FA	-15.97 (292 K) -28.89 (303 K) -35.20 (310 K)	299.42	1080.51
BSA-Chr	-30.28 (292 K) -21.83 (303 K) -24.10 (310 K)	-143.21	-390.30
BSA-Nar	-22.87 (292 K) -36.14 (303 K) -32.11 (310 K)	147.81	590.42
BSA-Kae	-40.38 (292 K) -36.30 (303 K) -24.74 (310 K)	-279.34	-813.51
BSA-Que	-26.83 (292 K) -38.52 (303 K) -32.11 (310K)	55.98	291.17

Energy transfer from BSA to PAs

Fluorescence resonance energy transfer (FRET) is a mechanism related to the transfer of energy between two chromophores that depends on their mutual distance. During protein-ligand interactions, the excitation energy is transferred from the donor/protein (BSA) to the acceptor/ligand (PAs or FLs), and the necessary conditions for this are: the donor molecule can produce fluorescence; the emission spectrum of the donor overlaps with the absorption spectrum of the acceptor; and the distance between the donor and the acceptor is less than 8 nm (Zhang, Zhou, Liu, *et al*., 2008). Based on FRET, the energy transfer efficiency (E) can be expressed as:

$$E = 1 - \frac{F}{F_0} = \frac{R_0^6}{R_0^6 + r^6} \qquad (6)$$

where F and F_0 are the fluorescence intensities of the donor after and before acceptor binding, r is the distance of the acceptor from the donor, R_0 is the critical distance at E = 50% which can be calculated as:

$$R_0^6 = 8.8\times10^{23}\ [\kappa^2 n^{-4} \Phi J(\lambda)] \qquad (7)$$

where κ^2 is the orientation factor between donor and acceptor (2/3), n is the refractive index of the medium (1.334) and Φ is the quantum yield of the donor (0.15). The spectral overlap integral (J) of the donor emission spectrum and the acceptor absorption spectrum is given as:

$$J(\lambda) = \int_0^\infty F(\lambda)\varepsilon(\lambda)\lambda^4\, d\lambda \qquad (8)$$

where $F(\lambda)$ and $\varepsilon(\lambda)$ are the fluorescence intensity of the donor and the molar absorption coefficient of the acceptor at the wavelength λ, respectively (Jayabharathi, Thanikachalam and Perumal, 2012). The overlap of the BSA fluorescence emission and *p*HBA absorption spectra are represented in Figure 3, while the summarized FRET results for all BSA-PAs/FLs pairs are given in Table 3. In all cases, the distance of BSA from the PAs/FLs is less than 8 nm, which indicates a high possibility of energy transfer from BSA to ligands how the resulting distance was obtained with great accuracy using FRET theory. Additionaly, it could be further confirmed PAs quenched BSA fluorescence in the manner of the static quenching due to $r > R_0$ (Phopin Ruankham, Prachayasittikul *et al*., 2020).

Synchronous and three-dimensional fluorescence spectroscopic studies

To explain the structural changes to BSA resulting from the addition of selected PAs or FLs, synchronous and 3D fluorescent spectra were recorded. These spectra provide information about the molecular environment near the chromophore. When the $\Delta\lambda$ value is stabilized at 15 and 60 nm, the synchronous fluorescence spectra give characteristic information of Tyr and Trp residues (Liu, Huang, Zhong, *et al*., 2018). The effect of selected PAs/FLs is shown in Table 4.

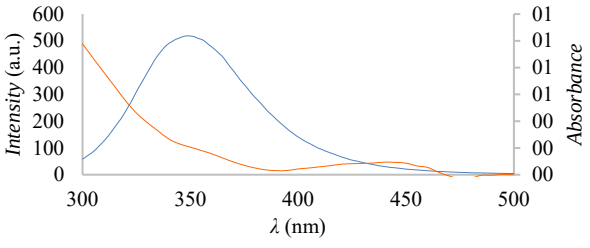

Figure 3: Overlap between emission spectrum of BSA and absorption spectrum of *p*HBA.

Table 3: BSA-PAs/FLs energy transfer parameters at 292 K.

#	J (cm^3 M^{-1})	R_0 (nm)	E	r
BSA-SA	3.347E-15	2.129	0.170	2.773
BSA-*p*HBA	3.021E-15	2.093	0.259	2.493
BSA-CA	8.133E-15	2.468	0.391	2.657
BSA-FA	5.652E-15	2.323	0.279	2.721
BSA-Chr	9.372E-15	2.527	0.701	2.193
BSA-Nar	5.309E-15	2.299	0.514	2.277
BSA-Kae	3.132E-14	3.090	0.802	2.448
BSA-Que	2.526E+14	2.981	0.844	2.250

Table 4: Shifts in synchronous fluorescence spectra

PAs	Δλ		FLs	Δλ	
	15 nm	60 nm		15 nm	60 nm
SA	2 nm (284→286)	1 nm (279→278)	**Chr**	5 nm (284→289)	2 nm (279→281)
***p*HBA**	3 nm (284→287)	0 nm	**Nar**	2 nm (284→282)	0 nm
CA	3 nm (284→287)	1 nm (279→278)	**Kae**	2 nm (284→282)	0 nm
FA	3 nm (284→287)	0 nm	**Que**	2 nm (284→282)	2 nm (279→281)

The emission wavelength of the Tyr residue is red-shifted in all cases for PAs and for Chr. This red shift indicates that the conformation of BSA was changed and it suggests a more polar (or less hydrophobic) environment for Tyr residue. At the same time, all additions of selected PAs/FLs cause a minor significat change shift in the fluorescence intensity of Trp residues in the position of the maximum (a minor blue shift was observed in the cases of CA and SA and a minor red shift was observed in the cases of Chr and Que). This suggests that the samples do not cause significant changes in the microenvironment of Trp residues. A possible explanation for the above lies in the fact that Tyr, unlike Trp, contains an aromatic OH group that can dissociate in the excited state, allowing easier binding and quenching of fluorescence (Jayabharathi *et al.*, 2012).

Three-dimensional spectra for BSA were also obtained in the absence/presence of selected PAs/FLs, and there two peaks were observed (Peak I, $\lambda_{ex}/\lambda_{em}$: 225/340 nm and Peak II, $\lambda_{ex}/\lambda_{em}$: 275/340 nm). While Peak I denotes the fluorescence spectral features of the polypeptides present in BSA and are due to π–π* transition of the polypeptide structures, Peak II is because of the existence of Tyr and Trp residues (Zhang *et al*., 2008). Except for SA for which the results of conformational changes are not clear, according to contour plots (Figure 4) in all cases, there is an increase in polarity in the Tyr and Trp microenvironment. Besides, a decrease and displacement of the Peak I suggest that PA addition to BSA might have decreased its diameter by interacting with the polypeptide residues, reflecting a conformational change in BSA (Wani, AlRabiah, Bakheit, *et al*., 2017). The changes in Peak I were also observed in the interaction of albumin with flavonoids, in particular with quercetin and kaempferol. The obtained results of conformational changes of BSA are in agreement with already published studies on structurally similar phenolics such as cinnamic acid, ferulic acid, caffeic acid, and chlorogenic acid (He, Liang, Luo, *et al*., 2010; Li, *et al*., 2010).

Thermal denaturation

The measuring principle of advanced differential scanning fluorimetry (nanoDSF) is an increasing temperature profile followed by changes in the intrinsic fluorescence of a protein. Destabilizing chemical or thermal influences might lead to changes in a protein and hence to changes in fluorescence intensities as well as shifts in unfolding transition temperature (T_m). In most cases, the loss of protein stability correlates with a reversible or irreversible unfolding often followed by an aggregation process. According to Figure 5, T_m values for BSA complexes with PAs, Nar and Que are slightly lower than T_m for BSA. The complexes BSA with Kae and Chr showed higher Tm values than BSA.

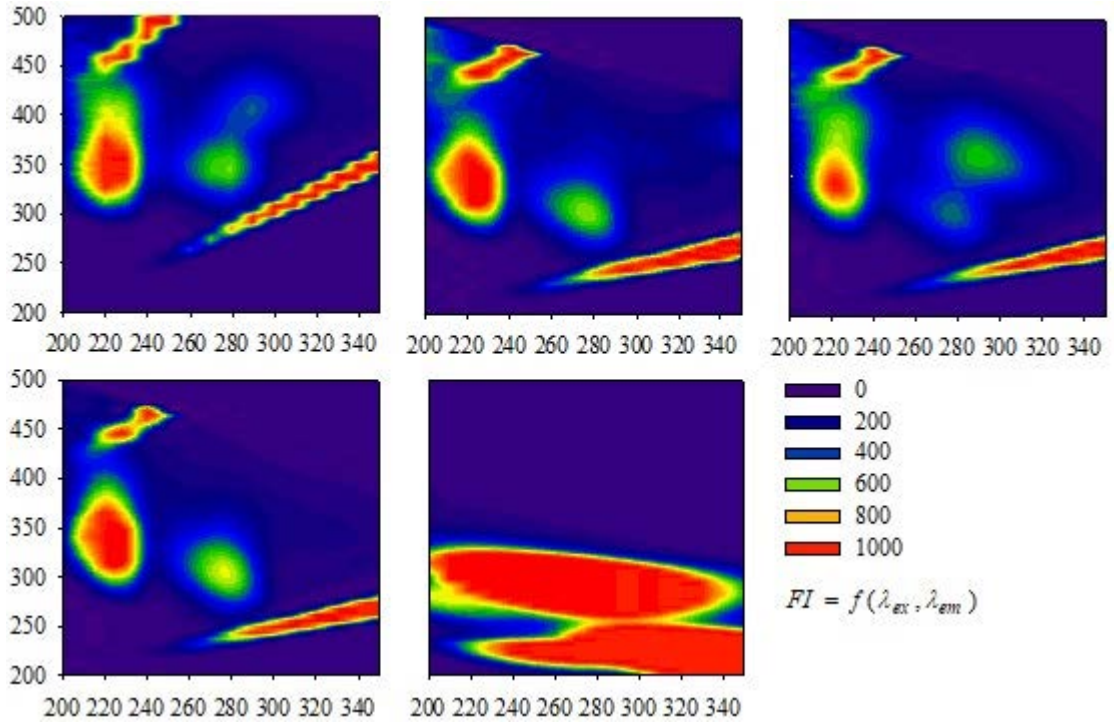

Figure 4: 3D fluorescence spectra. (a) BSA, (b) BSA-CA, (c) BSA-FA, (d) BSA-*p*HBA, and (e) BSA-SA

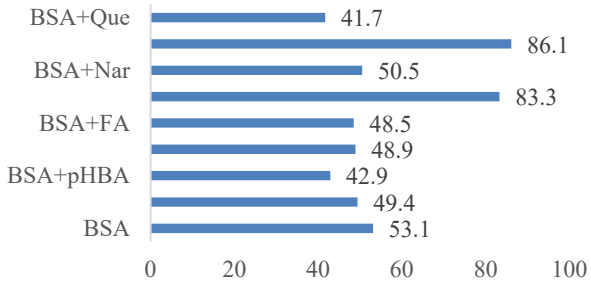

Figure 5: nanoDSF measurement. Unfolding transition temperature (*T*m, °C) values for BSA and BSA with PAs.

It should also be kept in mind that ligands can interplay with both the folded and unfolded states of target proteins, and a negative shift in melting temperature does not exclude binding to the native state (Gao, Oerlemans, Groves, 2020).

Molecular docking

Molecular docking is a widely used approach for modeling interactions between small compounds and macromolecules, including BSA, at the atomic level, which enables the characterization of the behavior of compounds at the binding site of target macromolecules (Cheng, Wang, Tang, et al., 2019).

The electronic structure of the ligand was investigated using a DFT modeling study. Relevant energetic properties such as the dipole moment (D) and energy were calculated for each compound (Table 5). Frontier molecular orbitals (FMO) predict the chemical reactivity of the lignand and identify the most likely reactive sites. The calculated energies of HOMO and LUMO help to explain the global reactivity descriptors (chemical hardness, chemical potential, and electrophilicity). The stability of the studied ligands was confirmed by the negative values obtained for their EHOMO and ELUMO (Yousef, El-Reash, El Morshedy, 2013).

The band energy gap correlates with the chemical reactivity and chemical stability of molecules. It was found that the energy difference [EHOMO-ELUMO] for Que is smaller than the band energy gap observed for other ligands, indicating greater reactivity. In contrast, the ligand *p*HBSA exhibited greater stability. An important parameter is the electrophilicity (ω) of the ligand, which evaluates its ability to accept electrons from its environment. The BSA selected for docking has an amino acid chain consisting of three homologous but structurally different domains (I, II and III), which are subdivided into nine loops by disulfide bonds and arranged in a heart-shaped molecule. Each of these domains consists of two subdomains, A and B. Molecular docking calculations were performed to determine the most probable binding site for the individual PAs and FLs in BSA and to identify the major amino acid residues and intermolecular forces involved in the interaction. The best-bound compound (with higher binding affinity for the protein) was revealed to be lidands Chr and Que. The docking pose for the best-bound ligand from PAs (BSA-SA) and from FLs (BSA-Que) is illustrated in Figure 6.

Table 5: Shifts in synchronous fluorescence spectra.

	E_{HOMO}	E_{LUMO}	*I*	*A*	Δ*E*	η	χ	μ	σ	ω	*D*	*E* (kJ/mol)
CA	-5.575	-1.568	5.575	1.568	4.007	2.004	3.572	-3.572	0.499	12.778	2.274	-2549.817
FA	-5.545	-1.449	5.545	1.449	4.096	2.048	3.497	-3.497	0.488	12.523	1.891	-5862.934
*p*HBA	-6.276	-0.902	6.276	0.902	5.374	2.687	3.589	-3.589	0.372	17.306	2.388	-2064.243
SA	-6.230	-1.013	6.230	1.013	5.217	2.609	3.622	-3.622	0.383	17.106	4.628	-2064.212
Kae	-4.954	-1.003	4.954	1.003	3.951	1.976	2.979	-2.979	0.506	8.763	-	-4281.861
Chr	-5.883	-1.456	5.883	1.456	4.427	2.214	3.670	-3.670	0.452	14.903	5.561	-3665.790
Que	-5.075	-1.417	5.075	1.417	3.658	1.829	3.246	-3.246	0.547	9.636	3.814	-4594.991
Nar	-5.734	-0.916	5.734	0.916	4.818	2.409	3.325	-3.325	0.415	13.317	3.391	-3973.851

I-ionization potential; *A*-electron affinity; Δ*E*-energy gap; η-global hardness; χ -electronegativity; μ-chemical potential; σ-global softness; ω-electrophilicity, *D*-dipole moment; *E*-energy

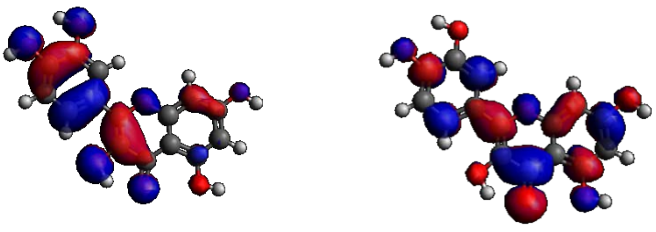

HOMO orbitals LUMO orbitals

Figure 5: Optimized structure of quercetin.

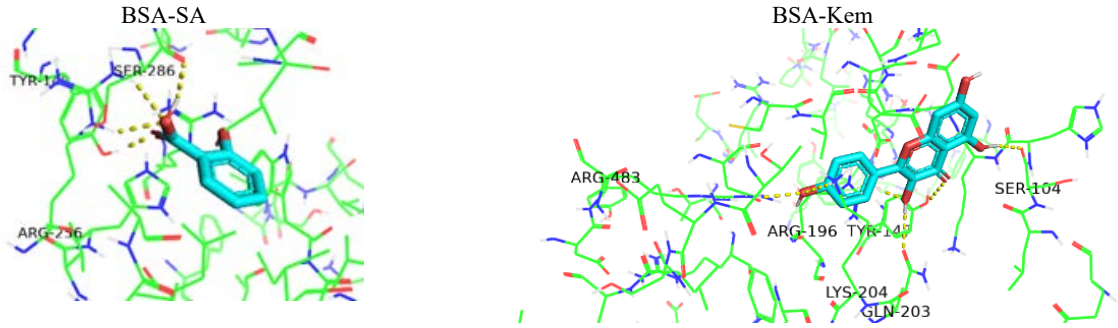

Figure 6: The complex BSA-SA and BSA-Kae as viewed in PyMOL.

The results obtained are summarized in Table 6, where a more negative affinity value indicates a stronger binding of the tested PAs/FLs to BSA and correlates with the H-bonds obtained.

Table 6: Hydrogen bonds in BSA (4F5S) interaction with selected PAs and FLs.

Sample	Affinity (kcal/mol)	Bonding in AChE/Distance (Å)
CA	-6.4	***H***-Lys132 → ***O***-[C4-OH] / 2.4 Å
FA	-6.3	***H***-Tyr137 → ***O***-[C1-O] / 2.0 Å
*p*HBA	-5.7	***H***-Arg208 → ***O***-[C1-OH] / 2.4 Å
SA	-5.6	***H***-[C1-OH] → ***O***-Ser286 / 2.1 Å ***H***-Tyr149 → ***O***-[C1-O] / 2.1 Å ***H***-Arg256 → ***O***-[C1-OH] / 2.2 Å ***H***-Arg256 → ***O***-[C1-OH] / 2.4 Å
Kem	-7.4	***H***-Arg196 → ***O***-[C3-OH] / 1.9 Å ***H***-Arg483 → ***O***-[C4'-OH] / 2.3 Å ***H*** [C5-OH] → ***O***-Ser104 / 2.3 Å ***H*** [C3-OH] → ***O***-Gln203 / 2.4 Å ***H***-Lys204 → ***O***-[C3-OH] / 2.3 Å ***H***-Tyr147 → ***O***-[C4-O] / 3.2 Å
Chr	-8.2	***H***-Tyr137 → ***O***-[C7-OH] / 2.8 Å
Nar	-7.9	***H***-[C7-OH] → ***O***-Glu125 / 2.3 Å ***H***-Lys116 → ***O***-[C4-O] / 2.7 Å
Que	-8.2	***H***-Lys136 → ***O***-[C4'-OH] / 2.2 Å ***H***-Lys132 → ***O***-[C3'-O] / 2.7 Å ***H***-Tyr160 → ***O***-[C4-O] / 3.1 Å

According to the results obtained, CA shows the strongest binding (affinity -6.4 kcalmol^{-1}) and binds with one H-bond (Lys132) and Que (affinity -8.2 kcalmol^{-1}) with three H-bonds (Lys132, Lys136 and Tyr160). All predicted binding sites are already proven sites of excellent binding and transport of bioactive compounds such as (*S*)-ibuprofen and (*S*)-ketoprofen (subdomain IA), while it is known that the active metabolite of nabumetone, 6-methoxy-2-naphtylacetic acid, binds similarly as CA in subdomain IIIA (Czub, Handing, Venkataramany, *et al*., 2020).

CONCLUSIONS

All PAs and FLs quenched the Trp fluorescence of BSA mainly by static quenching mechanism and thus showed the formation of non-fluorescent BSA-PAs/FLs complexes. The binding constant and binding site number depend on the number and position of hydroxyl groups in the molecules of phenolics. All interactions between PAs/FLs and BSA were spontaneous processes, hydrogen and hydrophobic bonds were the main acting force. The results of synchronous and 3D fluorescence spectroscopy indicate conformational changes in the structure of BSA in all BSA-phenolics systems, while the results of molecular docking support and correlate well with *in vitro* assays. Overall, the presented results imply that PAs/FLs could be stored and transported by BSA which may influence their biological and pharmacological activities in organisms.

ACKNOWLEDGEMENT

Authors are grateful for the financial support of the project by the Ministry of Science, Higher Education and Youth, Canton Sarajevo (27-02-1141251-18/21).

REFERENCES

Bartolomé, B., Estrella, I., Hernandez, M. T. (2000). Interaction of low molecular weight phenolics with proteins (BSA). *Journal of food science*, *65(4),* 617-621.

Bautista-Aguilera, O. M., Esteban, G., Bolea, I., Nikolic, K., Agbaba, D., Moraleda, I., Iriepa, I., Samadi, A., Soriano, E., Uzdeta, M., Marco-Contelles, J. (2014). Design, synthesis, pharmacological evaluation, QSAR analysis, molecular modeling and ADMET of novel donepezil-indolyl hybrids as multipotent cholinesterase/monoamine oxidase inhibitors for the potential treatment of Alzheimer's disease. *European journal of medicinal chemistry*, *75*, 82-95.

Bhattacharya, A. A., Grüne, T., Curry, S. (2000). Crystallographic analysis reveals common modes of binding of medium and long-chain fatty acids to human serum albumin. *Journal of molecular biology*, *303(5),* 721-732.

Bose, A. (2016). Interaction of tea polyphenols with serum albumins: A fluorescence spectroscopic analysis. *Journal of luminescence*, *169*, 220-226.

Bujacz, A. (2012). Structures of bovine, equine and leporine serum albumin. *Acta Crystallographica Section D: Biological Crystallography*, *68(10),* 1278-1289.

Cheng, D., Wang, X., Tang, J., Zhang, X., Wang, C., Li, H. (2019) Characterization of the binding mechanism and conformational changes of bovine serum albumin upon interaction with aluminum-

maltol: a spectroscopic and molecular docking study. *Metallomics*, *11*(*10*), 1625-1634.

Cui, C., Yan, S., Cai, B., Yao, X. (2002). Carbazole alkaioids as new cell cycle inhibitors and apoptosis inducers from *Clausena dunniana* Levl. *Journal of Asian natural products research*, *4(4),* 233-241.

Czub, M. P., Handing, K. B., Venkataramany, B. S., Cooper, D. R., Shabalin, I. G., Minor, W. (2020) Albumin-based transport of nonsteroidal anti-inflammatory drugs in mammalian blood plasma. *Journal of medicinal chemistry*, *63(13),* 6847-6862.

DeLano, W. L. (2002). Pymol: An open-source molecular graphics tool. *Collaborative Computational Project No. 4 on Protein Crystallography*, *40*(*1*), 82-92.

Gao, K., Oerlemans, R., Groves, M. R. (2020). Theory and applications of differential scanning fluorimetry in early-stage drug discovery. *Biophysical reviews*, *12(1),* 85-104.

He, T., Liang, Q., Luo, T., Wang, Y., Luo, G. (2010) Study on interactions of phenolic acid-like drug candidates with bovine serum albumin by capillary electrophoresis and fluorescence spectroscopy. *Journal of solution chemistry*, *39(11),* 1653-1664.

He, X. M., Carter, D. C. (1992). Atomic structure and chemistry of human serum albumin. *Nature*, *358(6383),* 209-215.

Jayabharathi, J., Thanikachalam, V., Perumal, M. V. (2012) A study on the binding interaction between the imidazole derivative and bovine serum albumin by fluorescence spectroscopy. *Journal of luminescence*, *132(3),* 707-712.

Jin, X. L., Wei, X., Qi, F. M., Yu, S. S., Zhou, B., Bai, S. (2012). Characterization of hydroxycinnamic acid derivatives binding to bovine serum albumin. *Organic & biomolecular chemistry*, *10(17),* 3424-3431.

Kacem, M., Kacem, I., Simon, G., Mansour, A. B., Chaabouni, S., Elfeki, A., Bouaziz, M. (2015). Phytochemicals and biological activities of *Ruta chalepensis* L. growing in Tunisia. *Food bioscience*, *12*, 73–83.

Lakowicz, J. R. (2013). *Principles of fluorescence spectroscopy*. (2ed Ed) Springer science & business media.

Li, S., Huang, K., Zhong, M., Guo, J., Wang, W. Z., Zhu, R. (2010) Comparative studies on the interaction of caffeic acid, chlorogenic acid and ferulic acid with bovine serum albumin. *Spectrochimica acta part A: Molecular and biomolecular spectroscopy*, *77(3),* 680-686.

Lloyd, J. B. F., Evett, I. W. (1977). Prediction of peak wavelengths and intensities in synchronously excited fluorescence emission spectra. *Analytical chemistry*, *49(12),* 1710-1715.

Magnusson, A. O., Szekrenyi, A., Joosten, H. J., Finnigan, J., Charnock, S., Fessner, W. D. (2019). nanoDSF as screening tool for enzyme libraries and biotechnology development. *The FEBS journal*, *286(1),* 184-204.

Mabry, T., Markham, K. R., Thomas, M. B. (2012). *The systematic identification of flavonoids*. Springer Science & Business Media.

Naveenraj, S., Anandan, S. (2013). Binding of serum albumins with bioactive substances–nanoparticles to drugs. *Journal of photochemistry and photobiology C: Photochemistry reviews*, *14*, 53-71.

Neese, F. (2022). Software update: The ORCA program system-Version 5.0. *Wiley Interdisciplinary Reviews: Computational Molecular Science*, *12*(5), e1606.

Ng, K. R., Lyu, X., Mark, R., Chen, W. N. (2019). Antimicrobial and antioxidant activities of phenolic metabolites from flavonoid-producing yeast: Potential as natural food preservatives. *Food Chemistry*, *270*, 123-129.

Peters, T. (1995). *All about albumin: biochemistry, genetics, and medical applications*. Academic press.

Phopin, K., Ruankham, W., Prachayasittikul, S., Prachayasittikul, V., Tantimongcolwat, T. (2020). Insight into the molecular interaction of cloxyquin (5-chloro-8-hydroxyquinoline) with bovine serum albumin: biophysical analysis and computational simulation. *International journal of molecular sciences*, *21*(1), 249.

Sudlow, G., Birkett, D. J., Wade, D. N. (1975). The characterization of two specific drug binding sites on human serum albumin. *Molecular Pharmacology, 11*, 824–832.

Tamba, M., Torreggiani, A. (2004). Radiation-induced effects in the electron-beam irradiation of dietary flavonoids. *Radiation Physics and Chemistry*, *71*(*1-2*), 23-27.

Trnkova, L., Bousova, I., Kubicek, V., Drsata, J. (2010). Binding of naturally occurring hydroxycinnamic acids to bovine serum albumin. *Natural science*, *2(6),* 563-570.

Trott, O., Olson, A. J. (2010). AutoDock Vina: improving the speed and accuracy of docking with a new scoring function, efficient optimization, and multithreading. *Journal of computational chemistry*, *31*(2), 455-461.

Vermerris, W., Nicholson, R. (2006). *Phenolic compound biochemistry*. Springer.

Wani, T. A., AlRabiah, H., Bakheit, A. H., Kalam, M. A., Zargar, S. (2017) Study of binding interaction of rivaroxaban with bovine serum albumin using multi-spectroscopic and molecular docking approach. *Chemistry central journal*, *11(1),* 1-9.

Wang, B., Qin, Q., Chang, M., Li, S., Shi, X., Xu, G. (2018). Molecular interaction study of flavonoids with human serum albumin using native mass spectrometry and molecular modeling. *Analytical and bioanalytical chemistry*, *410*, 827-837.

Yousef, T. A., El-Reash, G. A., El Morshedy, R. M. (2013). Structural, spectral analysis and DNA studies of heterocyclic thiosemicarbazone ligand and its Cr(III), Fe(III), Co(II) Hg(II), and U(VI) complexes. *Journal of Molecular Structure*, *1045*, 145-159.

Zahirović, A., Žilić, D., Pavelić, S. K., Hukić, M., Muratović, S., Harej, A., Kahrović, E. (2019). Type of complex–BSA binding forces affected by different coordination modes of alliin in novel water-soluble ruthenium complexes. *New journal of chemistry*, *43(15),* 5791-5804.

Zhang, Y. Z., Zhou, B., Liu, Y. X., Zhou, C. X., Ding, X. L., Liu, Y. (2008) Fluorescence study on the interaction of bovine serum albumin with *p*-aminoazobenzene. *Journal of fluorescence*, *18(1),* 109-118.

Zhao, Y., Chen, M., Zhao, Z., and Yu, S. (2015). The antibiotic activity and mechanisms of sugarcane (*Saccharum officinarum* L.) bagasse extract against food-borne pathogens. *Food Chemostry, 185*, 112–118.

Zeng, Y., Song, J., Zhang, M., Wang, H., Zhang, Y., Suo, H. (2020). Comparison of *in vitro* and *in vivo* antioxidant activities of six flavonoids with similar structures. *Antioxidants*, *9*(*8*), 732.

Zhu, T. T., Zhang, Y., Luo, X. A., Wang, S. Z., Jia, M. Q., Chen, Z. X. (2018). Difference in binding of long- and medium-chain fatty acids with serum albumin: The role of macromolecular crowding effect. *Journal of agricultural and food chemistry*, *66*(*5*), 1242-1250

Summary/Sažetak

U ovoj studiji korištene su tehnike fluorescencije za ispitivanja interakcija odabranih fenolnih kiselina (PA) i flavonoida (FL) s albuminom goveđeg seruma (BSA) pri fiziološkim uvjetima. Vezanje PA/FL s BSA ispitivano je na tri temperature: 292, 303 i 310 K. Iz dobivenih spektara nađene su: Stern-Volmerova konstanta (Ksv), bimolekularna konstanta gašenja (kq), konstanta vezanja (Kb) i broj vezivnih mjesta (n). Predstavljeni rezultati pokazuju da je gašenje fluorescencije BSA u prisutnosti fenolnih kiselina/flavonoida statički proces gašenja. Najjače statičko vezanje događa se tijekom stvaranja kompleksa BSA-*p*HBA (*p*-hidroksibenzojeva kiselina) (kq = 57,1×1012 M-1 s-1 pri 292 K), i BSA-Que (kvercetin) kompleksa (kq = 42,8× 1012 M-1 s-1 na 292 K). Otkriveno je da struktura PA/FL značajno utječe na proces vezanja/gašenja, a dodatno su studije prijenosa energije fluorescentne rezonancije potvrdile statičku prirodu ovog procesa. Rezultati spektra sinkrone fluorescencije ukazuju na promjene u mikrookruženju tirozina. Trodimenzionalni spektri pokazali su promjene povezane sa strukturama okosnice proteinskog lanca (uzrokovane prijelazom π-π∗ karbonilne skupine). Nadalje, toplinska denaturacija je provedena nano diferencijalnom skenirajućom fluorimetrijom (nanoDSF), a vrijednosti prijelazne temperature (T*m*) za BSA komplekse s PAs/FL su nešto niže od T*m* za BSA, osim T*m* za BSA komplekse s kamferolom i krizinom. Rezultati *in silico* analize pokazuju da kafena kiselina i kvercetin imaju najbolje vezivanje s albuminom (4F5S).